High pressure μSR studies: rare earths and related materials *

G.M. Kalvius [a], E. Schreier [a], M. Ekström [b], O. Hartmann [b], S. Henneberger [a], A. Kratzer [a], R. Wäppling [b], E. Martin [a], F.J. Burghart [a], R. Ballou [c], J. Deportes [c] and Ch. Niedermayer [d]

[a] *Physics Department, Technical University Munich, D-85747 Garching, Germany*
E-mail: kalvius@ph.tum.de
[b] *Physics Department, Uppsala University, S-75121 Uppsala, Sweden*
[c] *Laboratoire Louis Néel, CNRS, F-38042 Grenoble Cedex, France*
[d] *Faculty of Physics, University of Constance, D-78434 Konstanz, Germany*

After a short introduction to μSR with respect to the study of magnetic properties, followed by a brief outline of the principle of the high pressure–low temperature μSR spectrometer installed at the Paul Scherrer Institute, we discuss some measurements on rare earth materials employing this instrument. They are concerned with: (1) The pressure dependence of the spin turning process in ferromagnetic Gd. (2) The volume dependence of the internal magnetic field in the heavy rare earth metals Gd, Dy, and Ho in their ordered magnetic states. (3) The response of the (first order) magnetic transition in the frustrated antiferromagnets of type RMn_2 (R = Y,Gd) to pressure. (4) The variation of magnetic parameters with pressure in La_2CuO_4 (powder sample), the antiferromagnetic parent compound of the high T_C superconductors of type $La_{2-x}(Sr, Ba)_xCuO_4$. In conclusion a short outlook on further developments is given.

Keywords: muon spin rotation/relaxation, rare earth magnetism, frustrated magnets

1. Introduction

The understanding of the volume dependence of physical parameters is often the key to a deeper insight of electronic properties of solids. Theoretical treatments of electronic structure, such as band structure calculations, which have made enormous progress in recent years, render themselves more easily to predictions of trends with volume, than to the considerably more complex dependences on temperature. In addition, the measurement of pure temperature dependences is usually not possible due to the inherent coupling of volume to temperature. Corrections for true isochoric conditions require the knowledge of the appropriate volume coefficients. These reasons, together with the rapid advances in technology, are the main causes why high pressure

* Work supported in part by the BMBF, Germany (contract 03-KA4-TU1-9) and by the Swedish Science Research Council.

measurements have gained largely in importance during the last decade or so among the different spectroscopic techniques sensitive to the electronic state of matter.

The technique of Muon Spin Rotation and Relaxation (μSR) has become a valuable tool for the study of internal properties of magnetic materials. In particular, the often unexpected results obtained in the study of novel materials like heavy fermions [1] or high temperature superconductors [2] has brought widespread attention to μSR spectroscopy. μSR senses the magnitude and the time dependence of the magnetic field *between* the atoms (interstitial field). It differs in this respect fundamentally from other nuclear hyperfine methods, which measure the field at the nucleus (not necessarily of the atom carrying the moment). The nuclear field is in any case generated by its own electron shell. The properties of the interstitial field as determined by μSR can be related to the spatial and temporal properties of the spin system in a magnetic substance. In particular, μSR is a very sensitive probe for the detection of short-range ordered magnetism, for changes in the spin structure of ordered magnets such as spin re-orientations, and for the development of spin correlations, especially on approach to and within the critical region of a magnetic transition.

Changes of volume directly affect magnetic properties in most cases. The high sensitivity of μSR allows measurements at volume compressions of less than 1% where linear approximations are well valid. The restriction of the present μSR set-up (originally developed by the TU Munich–University of Uppsala collaboration [3]) to $\sim$10 kbar (1 GPa) is, hence, not a serious restriction from that point of view. Many interesting magnetic phase transitions occur, however, at higher pressures and from that point of view the restriction in pressure range is a handicap. Even more serious is the present limitation in temperature (either $\sim$12 or $\sim$5 K, depending on the cryogenic system used), especially when modern magnetic systems such as heavy fermions are to be studied. Still, the system in operation has produced a fair number of interesting and important results. In this report we discuss measurements by our collaboration which center on the rare earth metals and some of their intermetallic compounds. Other groups have also successfully used the apparatus. Their work includes studies of transition elements [4] and intermediate valence compounds [5].

2. Basics of μSR spectroscopy

We discuss briefly the elementary features of the application of *positive* muons to magnetism. Detailed information is available in several monographs on the subject (see, for example, [6,7]).

Muons are created in the decay of pions:

$$\pi^+ \rightarrow (\tau_\pi = 26\,\mathrm{ns}) \rightarrow \mu^+ + \nu_\mu. \tag{1}$$

These, in turn, are generated by proton–proton or proton–neutron collisions at medium high energies. One starts with an intense beam ($\sim$200 μA) of $\sim$800 MeV protons which impinges on a carbon or beryllium target. Such facilities are available, for

example, at the Paul Scherrer Institute (PSI) near Zürich, Switzerland (which was used for the high pressure studies), at the TRIUMF meson factory in Vancouver, Canada, at the ISIS neutron spallation source near Oxford, England and at BOOM located within the Japanese high energy laboratory (KEK) in Tsukuba. One may use either muons produced by pions which have come to rest in the production target near its surface ("surface muons"), or by pions ejected from the production target which then decay in flight ("decay muons"). The former are of low energy and have small penetration depths. This allows thin samples ($\sim$100 mg/cm^2) and they are nearly exclusively employed in standard μSR spectroscopy. In high pressure work they will not pass through the walls of the high pressure cell and one needs decay muons. The decay channel is often realized as $\sim$5 m long superconducting solenoid. To give the reader an impression of the machinery involved we show in figure 1 the outlay of the meson production facility at PSI. The high pressure spectrometer is located either at the μE4 or the μE1 stations in the central hall (details in figure caption).

Looking at eq. (1) while keeping in mind that the neutrino (ν_μ) has a definite helicity (i.e., its spin always points opposite to its momentum) and that the pion is spinless leads to a fixed orientation of the muon spin opposite to the direction of its linear momentum as a consequence of momentum conservation in the pion rest frame. For surface muons this is also the laboratory frame. For decay muons one has to perform a Lorentz transformation into the laboratory frame. One finds that the orientation of muon spins depends on the direction of ejection of the muon with respect to pion travel direction. Relativistic kinematics always results in a muon traveling in the direction of pion momentum but the muon spin is parallel to muon momentum for forward emission or antiparallel for backward emission. In any case the muon beam is nearly 100% spin polarized. Backward decay muons have a more favorable energy range and were nearly exclusively used in the measurements to be discussed.

The beam of polarized muons impinges onto the sample. The implanted muons are quickly thermalized (in less than 1 ns) and, due to their positive charge, come to rest at an interstitial lattice site. At least in conducting materials their spin polarization is fully maintained in the stopping process. One should further realize that disturbances of lattice structure by radiation damage occur mainly at the beginning of the muon track. The vicinity of the stopping site is not damaged. General radiation damage by total dose is negligible. The result is that we have a polarized probe spin ($\vec{S}_\mu = 1/2$) inside the sample without the need of applying a magnetic field (in contrast to standard NMR). The stopping site is *a priori* not known. It can be determined by special μSR experiments or deduced from hydrogen loading data. For many applications of μSR to magnetism, the exact knowledge of the muon site is not essential. It is more crucial to make sure, again by appropriate μSR experiments, that the muon rests over its lifetime at one specific site. Muon diffusion is a possibility, but at low temperatures it usually is observed only in pure cubic elemental metals such as Cu. In the rare earth and their intermetallics it poses in general no problem for magnetic studies.

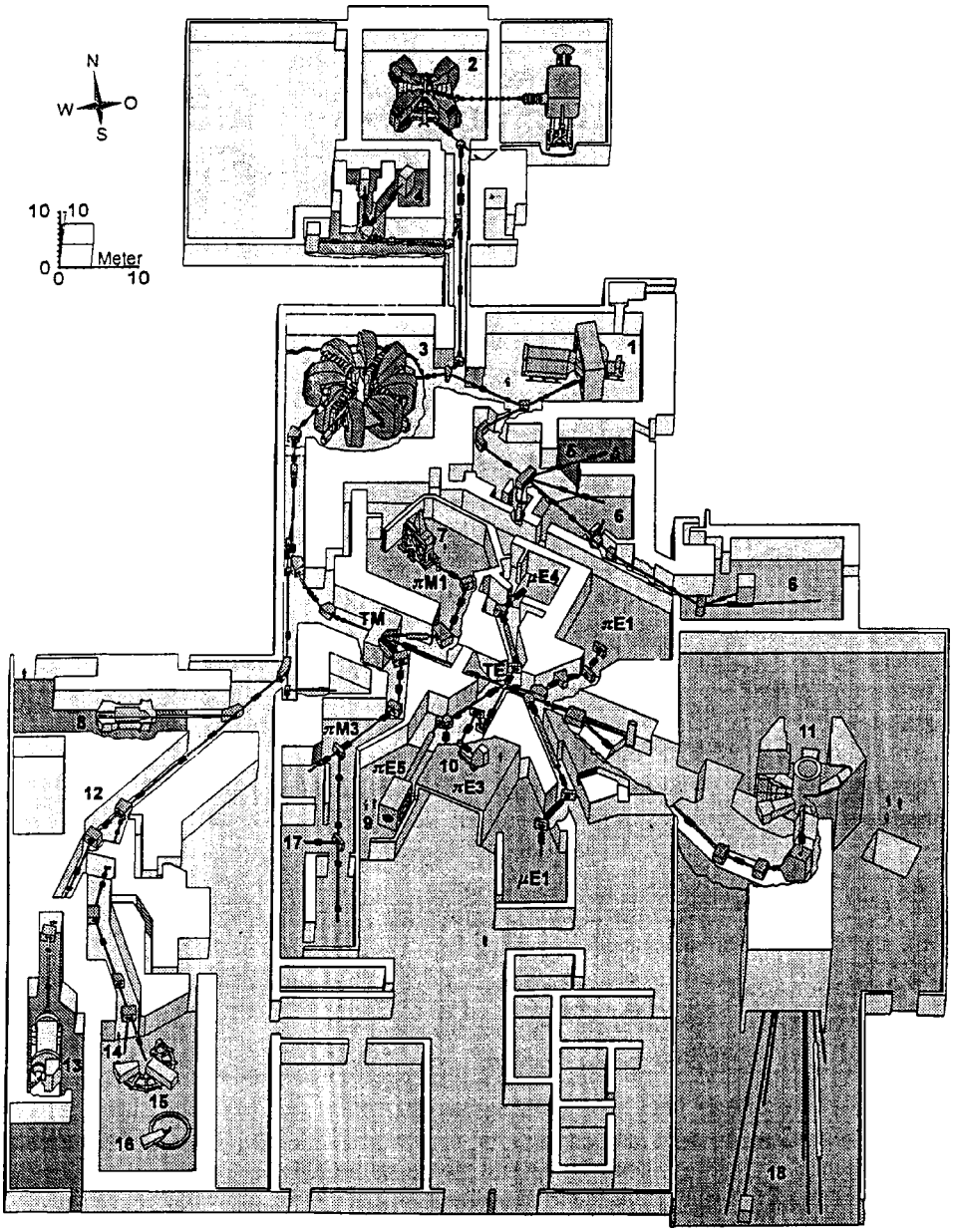

Figure 1. Layout of the meson facility at the Paul Scherrer Institut (PSI) in Switzerland. The pre-injector and injector (2) feed a proton beam to the main accelerator, the sector cyclotron (3). The 590 MeV, 1.5 mA proton beam passes through two pion production targets (TM and TE) in the central hall and ends at the neutron spallation target (11) to the right. Surface muons for μSR studies are available at station πM3. The ports μE1 and μE4 have superconducting pion decay channels. They provide the decay muons needed for high pressure μSR. The left hall (12–16) is used for research with protons including a medical irradiation facility. The right hall contains the neutron spallation source SINQ (11 and 18) with its neutron guides. (Picture courtesy of PSI public relations office.)

The muon has a mean life of 2.2 μs and decays into a positron and two neutrinos:

$$\mu^+ \rightarrow (\tau_\mu = 2.2\ \mu\text{s}) \rightarrow e^+ + \nu_e + \bar{\nu}_\mu. \tag{2}$$

Due to parity violation in weak interaction the positron is preferentially emitted along the direction of the muon spin, leading to an asymmetric angular distribution of positrons:

$$W(\theta) = 1 + a_0 \cos\theta. \tag{3}$$

Here θ is the angle between spin direction and path of travel of the positron and a_0 is the "initial asymmetry". Its theoretical value is $\frac{1}{3}$; under normal experimental conditions one usually finds numbers around 0.2. Positron detectors placed in front and at the back (with respect to the muon beam) measure an asymmetry in rate N of decay positrons:

$$A = \frac{N_{\text{forw}} - N_{\text{backw}}}{N_{\text{forw}} + N_{\text{backw}}}. \tag{4}$$

If the muon spin were stationary, one would observe in a time differential measurement of count rate just the decay rate of the muon in each detector (e.g., $N_{\text{forw}} = a_0 \exp[-\tau_\mu t]$) which cancels if the count rate asymmetry according to eq. (4) is formed. The result is a time independent asymmetry $A = a_0$ which is of no particular interest. If the muon senses a magnetic field $\vec{B}_\mu$ at its interstitial site, then the muon spin will precess around the field axis. It takes with it the positron emission distribution $W(\theta)$ resulting in a temporal modulation of count rates in the positron detectors. In the simplest case one now gets for the count rate asymmetry (applying eq. (4)):

$$A(t) = a_0 \cos(2\pi\nu t), \tag{5}$$

where the precession frequency is given by

$$\nu = \frac{\gamma_\mu}{2\pi} B_\mu. \tag{6}$$

Here γ_μ is the muon gyromagnetic ratio ($\gamma_\mu = 2\pi \cdot 13.5$ MHz/kG). The large value of γ_μ makes μSR sensitive to rather small fields ($\sim$1 G). A plot of $A(t)$ vs. the time t elapsed since the implantation of the muon represents the μSR spectrum. It directly reflects the motion of the muon spin due to its coupling to the interstitial field B_μ. The detection of such a spectrum requires a time differential measurement of N_{forw} and N_{backw} and the formation (with some corrections) of $A(t)$ according to eq. (4). The basic outlay of an appropriate apparatus (μSR spectrometer) is shown in figure 2. For details we refer to the texts mentioned above. We shall discuss some typical cases of μSR response in magnets further below.

First, we treat the sources of the local field which is generally expressed as the vector sum of three terms:

$$\vec{B}_\mu = \vec{B}_{\text{c}} + \vec{B}_{\text{dip}} + \vec{B}_{\text{ext}}, \tag{7}$$

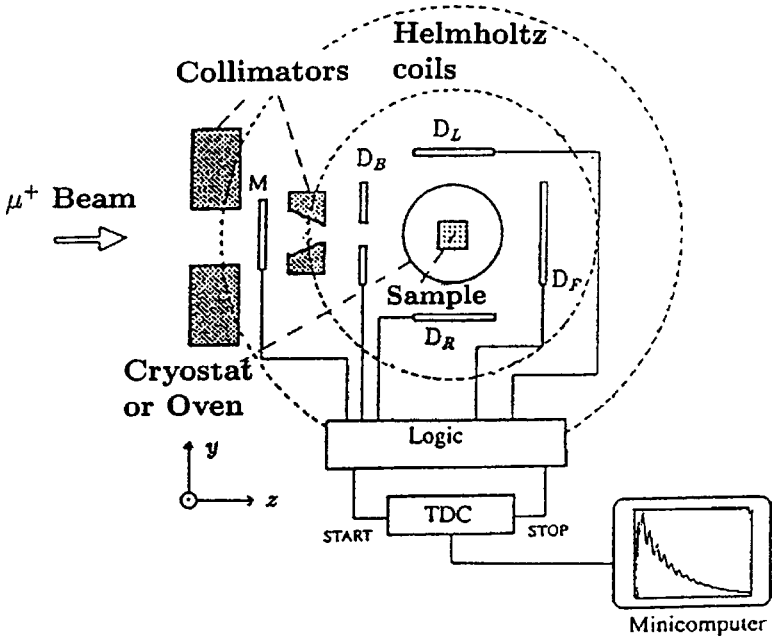

Figure 2. Schematic of a μSR spectrometer. The M counter starts the digital clock TDC which is stopped by the detection of a positron. The event is stored in the appropriate time bin thus creating a counts vs. time histogram. The spectrometer shown uses two pairs of positron detectors (backward ↔ forward and left ↔ right). In the high pressure spectrometer usually only backward↔forward detectors are used.

where B_{c} is the contact field from conduction electrons spin-polarized by the magnetic moments in the sample. Clearly, it is absent in insulators. In conductors one has to consider that the muon with its positive charge attracts a conduction electron cloud which causes a local enhancement of conduction electron density and with it of B_{c}. In rare earth materials an enhancement factor of 3 has been estimated [8]. B_{ext} is the applied field. B_{dip} is the dipolar field from surrounding magnetic moments (which might be influenced by B_{ext}). One often makes use of the Lorentz construction and writes

$$\vec{B}_{\mathrm{dip}} = \vec{B}'_{\mathrm{dip}} + \vec{B}_{\mathrm{L}} + \vec{B}_{\mathrm{D}}, \tag{8}$$

where B'_{dip} is the dipolar field within the Lorentz sphere, which has to be calculated by lattice sums. B_{L} is the Lorentz field (proportional to domain magnetization) and B_{D} the demagnetizing field (proportional to resultant sample magnetization). The moments to be considered as sources of B_{dip} can be either nuclear or electronic. Only the electronic moments are of real interest to us, but the effect of nuclear moments might have to be considered in the data analysis. One big bonus of μSR is that it can always be performed in true zero field (ZF). In this case only internal field sources exist and eqs. (7) and (8) reduce to

$$\vec{B}_{\mu} = \vec{B}_{\mathrm{c}} + \vec{B}'_{\mathrm{dip}} + \vec{B}_{\mathrm{L}}. \tag{9}$$

The dipolar field can be calculated by appropriate lattice sums with good accuracy, at least as long as the approximation of a local dipole moment holds. The contact field is difficult to handle theoretically. It requires the calculation of interstitial spin densities *in the presence of the muon*.

Let us now briefly discuss the characteristic μSR response to magnetism. We must stress that the following is often a gross simplification and should be considered an elementary guide line only.

In a paramagnet in ZF the magnetic moments are randomly oriented resulting in $\langle B_\mu \rangle = 0$. A muon spin precession pattern is not observed, but the orientational randomness causes a distribution $P(B_\mu)$ of the local field around $\langle B_\mu \rangle = 0$. One characterizes the width of the distribution by a parameter Δ (in frequency units), which in the case of a dense magnetic system is given by the second moment of the field $\langle B_\mu^2 \rangle$. The field distribution leads to depolarization of the muon spins and the μSR spectrum takes the form

$$A(t) = a_0 G_z(t), \tag{10}$$

where $G_z(t)$ is the longitudinal depolarization or relaxation function. The case under discussion has been treated by Kubo and Toyabe (see [9]). The result is presented in figure 3 with the (normalized) spin fluctuation time τ as parameter. The case $\tau = \infty$ relates to a spin frozen system and the time independent asymptote at late times $G_z(\Delta t \gg 1) = \frac{1}{3}$ is typical for static spins. Normal paramagnets, however, are in the fast dynamic limit $\Delta\tau \ll 1$. The relaxation function is then just a simple exponential decay of muon spin polarization: $G_z(t) = \mathrm{e}^{-\lambda t}$ with $\lambda = 2\Delta^2\tau$. In the static case one can suppress depolarization by the application of an external field along the initial muon spin orientation (beam axis). This is called a longitudinal field (LF) and its effect is shown in figure 4. One speaks of decoupling spectra. Establishing longitudinal field decoupling provides a most sensitive test for the presence of a static random spin

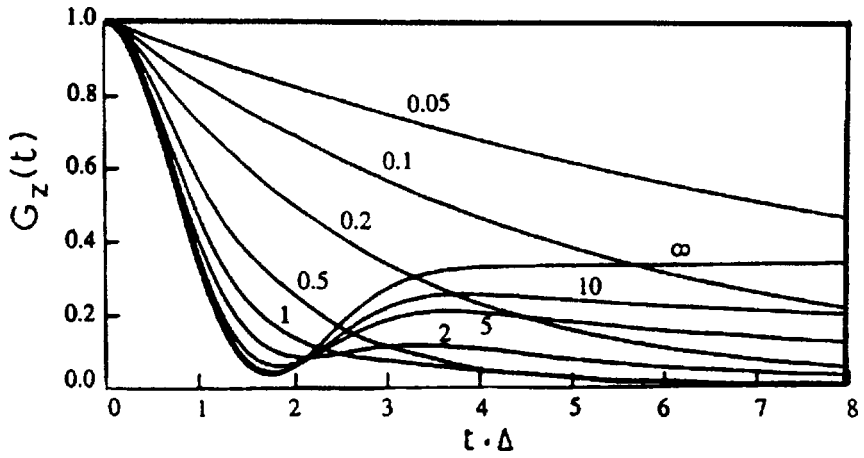

Figure 3. Gaussian Kubo–Toyabe relaxation function. The parameter is the spin fluctuation time in units of the field width Δ.

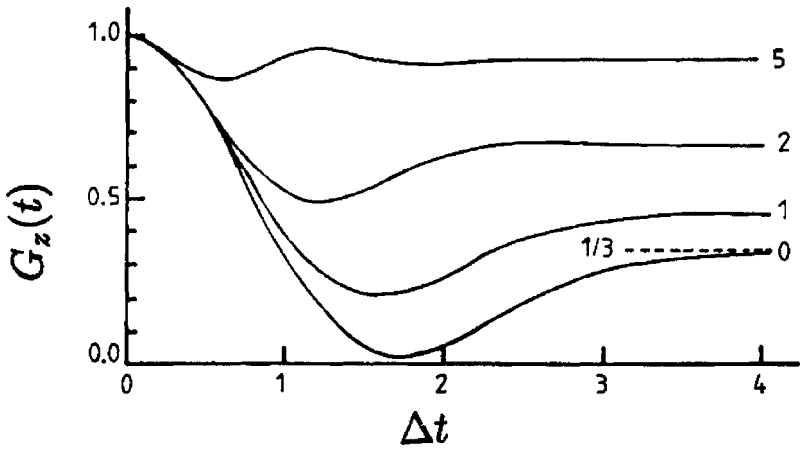

Figure 4. The influence of a longitudinal field on the Gaussian Kubo–Toyabe function in the static limit ($\tau \to \infty$). The parameter is the field strength in units of $\gamma_\mu B_{\rm LF}/\Delta$.

system. If an external field is applied transverse to muon spin polarization (TF), one observes a spin precession pattern, which, in the presence of fast spin fluctuations, can be expressed as

$$A(t) = a_0 \mathrm{e}^{-\lambda t} \cos(2\pi\nu t). \tag{11}$$

The important parameter is the precession frequency ν, which in general is shifted compared to the value $\nu_0 = (\gamma_\mu/2\pi)B_{\rm TF}$ corresponding to the pure externally applied transverse field. The cause is the additional action of the internal fields in a paramagnet (there is also a minute – and in majority of cases negligible – diamagnetic shift in metals caused by conduction electron polarization). This so-called muonic Knight shift $(\nu - \nu_0)/\nu_0$ is a measure of the interstitial susceptibility. An example of frequency shift is shown in figure 5. The factor $\mathrm{e}^{-\lambda t}$ damps out the oscillatory pattern and one calls λ the (muon spin) relaxation rate. It reflects spin motion in a paramagnet. Of particular interest is its behavior in the vicinity of a magnetic phase transition.

In long range ordered systems a more or less well defined local field is present at the muon site (i.e., $\langle B_\mu \rangle \neq 0$) which causes muon spin precession. In the case of a powder sample (without texture) the μSR spectrum is given by

$$A(t) = a_0 \left[\frac{2}{3} \mathrm{e}^{-\lambda_{\rm T} t} \cos(2\pi\nu t) + \frac{1}{3} \mathrm{e}^{-\lambda_{\rm L} t} \right]. \tag{12}$$

The two relaxation rates $\lambda_{\rm T}$ (transverse relaxation) and $\lambda_{\rm L}$ (longitudinal relaxation) contain different informations. Usually $\lambda_{\rm T}$ is dominated by the distribution of the local field due to imperfections of the spin lattice (or some disorder in the spin structure) and much larger than $\lambda_{\rm L}$, which in contrast, is solely sensitive to spin fluctuations. An example of a μSR spectrum corresponding to eq. (12) is shown in figure 6. In the quasistatic limit one has $\lambda_{\rm L} \to 0$, which should prevail in an ordered magnet for $T \to 0$. We use the term "quasistatic" because very fast dynamics such as spin wave excitations

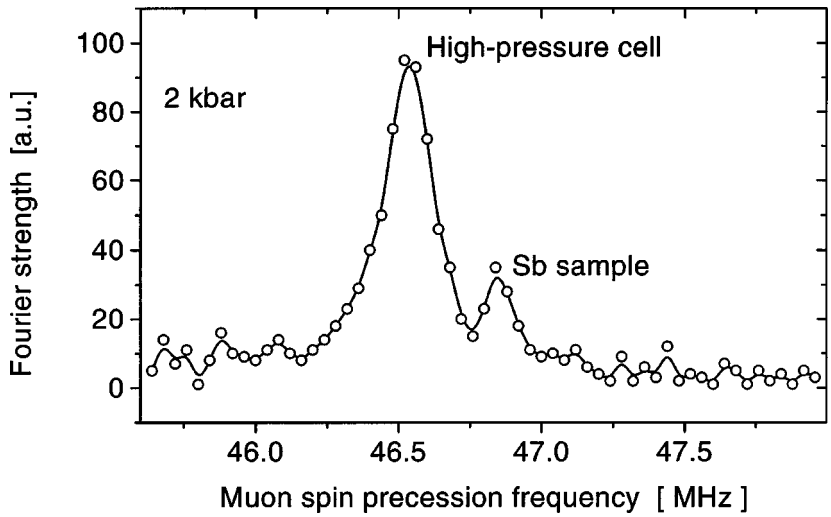

Figure 5. Fourier transform of the transverse field (3.5 kG) μSR spectrum of Sb metal in the high pressure cell at 2 kbar and 30 K. The spins of muons stopped in the cell walls precess with the unshifted frequency corresponding to the applied field. In contrast, the spins of muons stopped in the sample suffer a positive Knight shift (of $\sim$0.5%) in their precession frequency (after [10]).

may be present in the system. They are beyond the time window of μSR and are felt, as in all hyperfine methods, as a temperature variation of precession frequency $\nu(T)$ which in simple cases follows roughly the temperature dependence of bulk magnetization, i.e., has a Brillouin-like shape. Sometimes the relaxation rates in eq. (12) are so large that the muon spins depolarize in less than $\sim$1 ns and the μSR spectrum becomes unobservable due to limitations in time resolution of the spectrometer. That means, $a_0 \to 0$ for $T < T_{\mathrm{mag}}$ if T_{mag} is the magnetic transition temperature. This effect can be easily detected in TF measurements. For $T > T_{\mathrm{mag}}$ (paramagnetic regime) a spin precession pattern (with Knight shift) is observed. Around T_{mag} the signal strength rapidly decreases which serves as a convenient indicator of the magnetic transition. Such a procedure is often used to measure the pressure dependence of T_{mag}.

3. Basics of μSR high pressure experiments

μSR spectroscopy unfortunately can not be extended easily to high pressures. Whatever way pressure is applied, the beam must pass through a fair amount of material before reaching the sample. As stated, only decay channel muons can be used, which, in turn, demand fairly thick samples. Furthermore, it is important that hydrostatic conditions prevail, since internal stress in the sample will produce lattice defects which may trap muons and also can cause wide distributions in internal fields which then cause rapid depolarization of the muon spin. The most widely used Bridgeman opposed anvil technique is problematic for μSR spectroscopy.

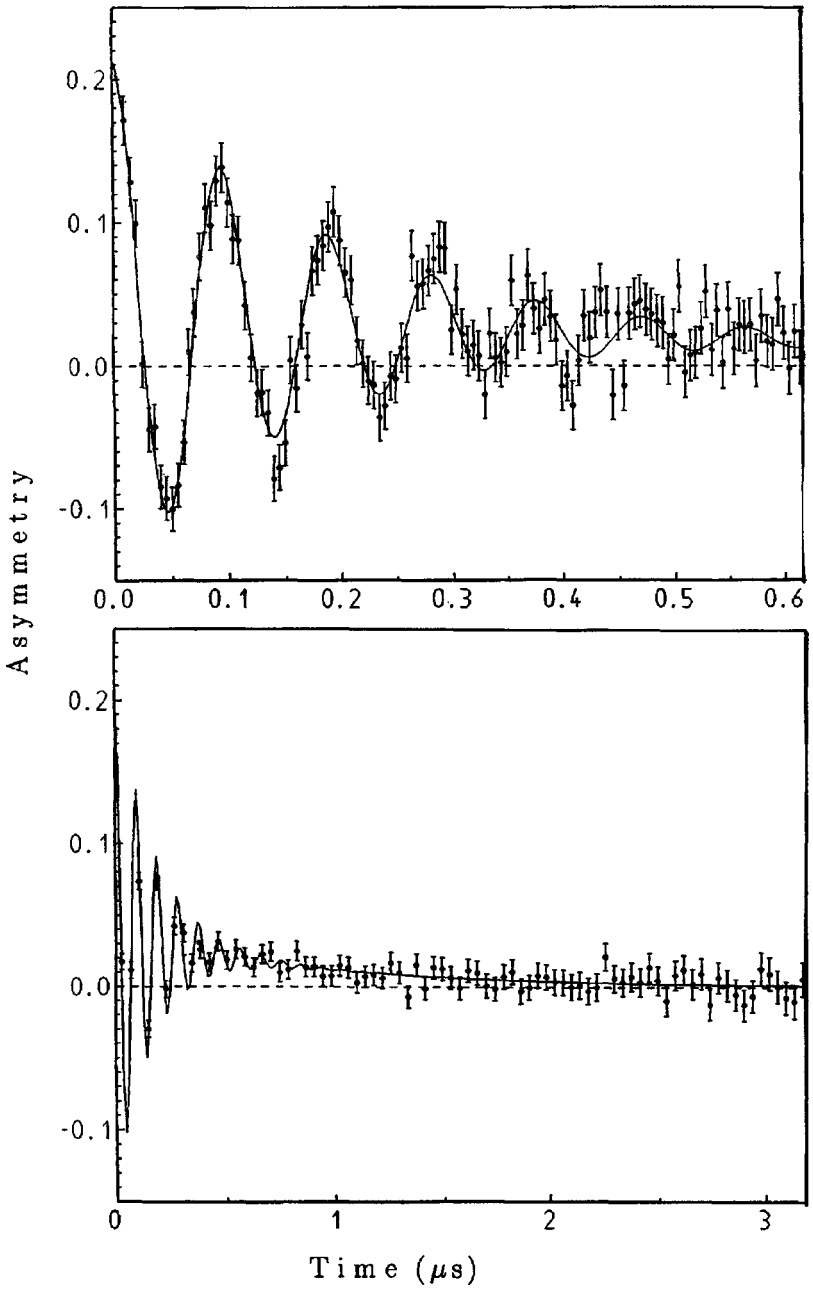

Figure 6. μSR spectrum of ferromagnetic Gd at ambient pressure and 235 K. The solid line is a least squares fit to eq. (12). The top panel shows details at early times, the bottom panel extends the spectrum to later times using a reduced grid of data points. The oscillatory term decays more rapidly than the non-oscillatory term ($\lambda_T = 5.5\ \mu s^{-1} > \lambda_L = 1\ \mu s^{-1}$). The ratio of intensity of the two terms deviates somewhat from the isotropic value 2 : 1 due to preferred orientation of the crystalline c-axis (easy axis of magnetization).

The easiest solution is an oil pressure cell. This has been used for the study of the volume dependence of the local field in the transition metals Fe and Ni [11]. The pressure range was 7 kbar. The most serious problem with such a system is the freezing of the pressure transmitting fluid (oil) even at moderately low temperature. Rare earth magnetism studies call for much lower temperatures which, under fully hydrostatic conditions, can only be achieved with a gas pressure cell. Highly compressed He gas is the optimal pressure transmitting medium and this type of apparatus, designed for pressures up to 14 kbar, is used in the present study. Details of the construction can be found in [3,12]. Helium solidifies in the low temperature–high pressure regime. Solid helium, fortunately, can not support significant shear forces and, consequently, the all important hydrostatic conditions are not seriously violated. A sketch of the system is shown in figure 7. Helium compression is achieved in two steps. First, the gas is

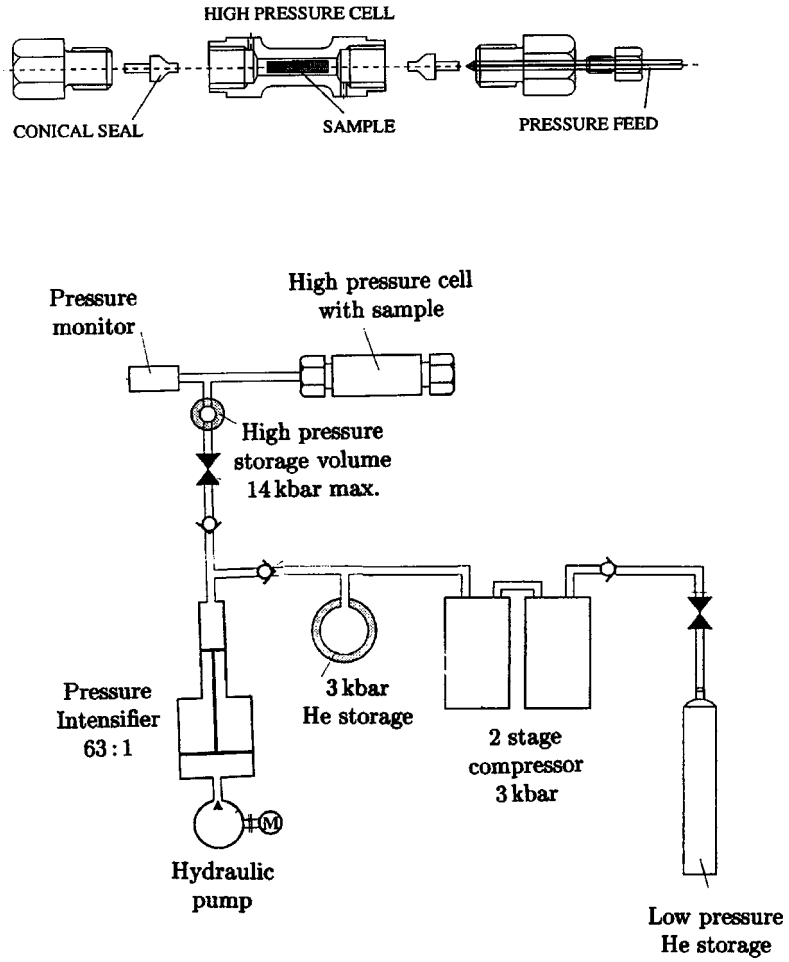

Figure 7. Schematic of the gas high pressure system (explanation in text). On top the high pressure cell of CuBe used in the rare earth studies is shown.

compressed to 3 kbar and stored. This is followed by a pressure intensifier, which is a piston system with an area ratio of 63 : 1, driven by a water-cooled hydraulic oil pump. The high pressure gas is fed to the high pressure cell located at the muon beam port. The high pressure gas storage guarantees stable pressure when changing the temperature. Therefore, after equilibration, the selected pressure is stable for several days.

The high pressure cell used recently for the study of rare earth materials is made from CuBe and contains a central bore of 7 mm in diameter and $\sim$70 mm length as sample space. It will withstand $\sim$9 kbar. It is cooled by a closed cycle refrigerator with a base temperature $\sim$12 K. The beam is directed perpendicular to the bore axis and collimated accordingly. Transverse fields were were originally generated by an electromagnet. Recently, water cooled Helmholtz coils have been installed to avoid the problems with hysteresis of the applied field. Weak longitudinal fields are available from a a pair of small Helmholtz air coils.

Even under favorable conditions, at least 50% of the μSR signal arises from the cell. A typical example of a raw spectrum is shown in figure 8. It is important that the sample and cell signal can be clearly separated. In transverse field measurements this requires a noticeable Knight shift of the sample precession frequency (as demonstrated in figure 5). In zero field one either needs spontaneous spin precession (ordered magnet, as depicted in figure 8) or a fairly rapidly depolarizing signal from the sample. The slow depolarization of muon spins stopped in the cell material can easily be suppressed

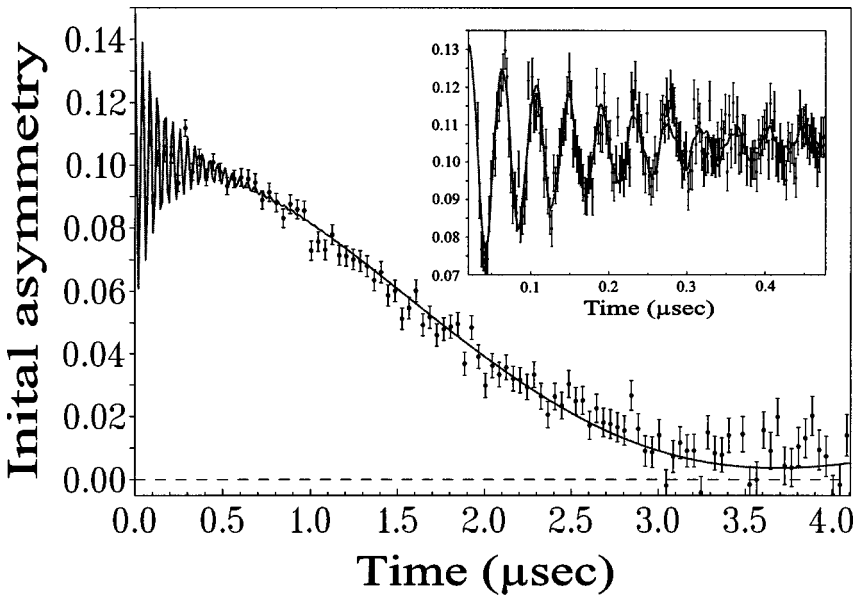

Figure 8. Typical ZF-μSR spectrum obtained with the high pressure spectrometer. The case is ferromagnetic Gd. Spontaneous spin precession produces the oscillatory pattern (see figure 6). This is the sample signal shown in the inset in more detail. The slowly depolarizing signal arises mainly from muons stopped in the cell walls (Kubo–Toyabe relaxation due to the field from Cu nuclear dipoles).

by weak LF. This is another means to separate the two signals, provided the sample signal is not affected by the field.

4. High pressure studies of rare earth metals

All high pressure measurements were carried out on single crystals. The samples were thin rods which tightly fitted into the bore of the high pressure cell. The c-axis was oriented parallel to the initial muon spin polarization for Dy and Ho (magnetic moments confined to the basal plane) and perpendicular to it in Gd.

4.1. Spin turning in ferromagnetic gadolinium

From a magnetic point of view, Gd is the simplest of the RE metals. Exchange favors ferromagnetism (FM) throughout, while all other heavy RE metals initially show antiferromagnetic (AFM) order. The Curie temperature of ($T_{\mathrm{C}} = 293$ K) is convenient, in particular for high pressure experiments. The Gd^{3+} ion has a half filled $4f$ shell. It is thus an S state ion featuring pure (but very strong) spin magnetism. CEF interactions vanish because of the S character. A small residual anisotropy causes the moments to point along the c-axis just below T_{C}. About 70 K lower, the easy axis begins to move out of the c-direction toward the basal plane. It is thought that this spin turning arises from the action of a competing anisotropy having its origin in spin–orbit coupling.

A clear muon spin precession signal is seen below T_{C}. Its temperature dependence is peculiar (see figure 9). It shows initially the Brillouin-type rise usually seen below a second-order transition, but marked deviations from that behavior occur when the temperature is further lowered. These deviations have their origin in the competition between the isotropic $\vec{B}_{\mathrm{c}}$ and the anisotropic $\vec{B}_{\mathrm{dip}}$, the latter being connected to the turning of spins. This effect is particularly noticeable in Gd because B_{c} and B_{dip} are of comparable magnitude. Using a tensor field formalism allows the safe separation of the contact and the dipolar contributions to the local field at the muon site [13,14]. Both polycrystalline samples and single crystals gave the same results, providing data on the temperature dependence of the spin tilt angle Θ and also identifying the muon stopping site as the octahedral interstitial position. The former is found to be in excellent agreement with other determinations [15–17]. The contact field for $T \rightarrow 0$ is -0.70 T. Also shown in figure 9 is the dependence on temperature of the relaxation rate λ_T. It peaks at the onset of spin turning, demonstrating that the spin system is in disorder at this point.

The temperature dependence of the precession frequency (i.e., the field at the muon site) is highly sensitive to applied pressures even in the fairly low pressure range up to 6 kbar. The dominant reason is the dependence of the spin turning process on pressure. The findings are summarized in figure 10. Under hydrostatic pressure the onset of spin-turning gradually shifts from 230 K to lower temperatures and also T_{C} decreases slightly, but with a lower rate. In addition, the turn angle Θ gets larger with pressure below 170 K. At 6 kbar it attains 90° over the full temperature interval

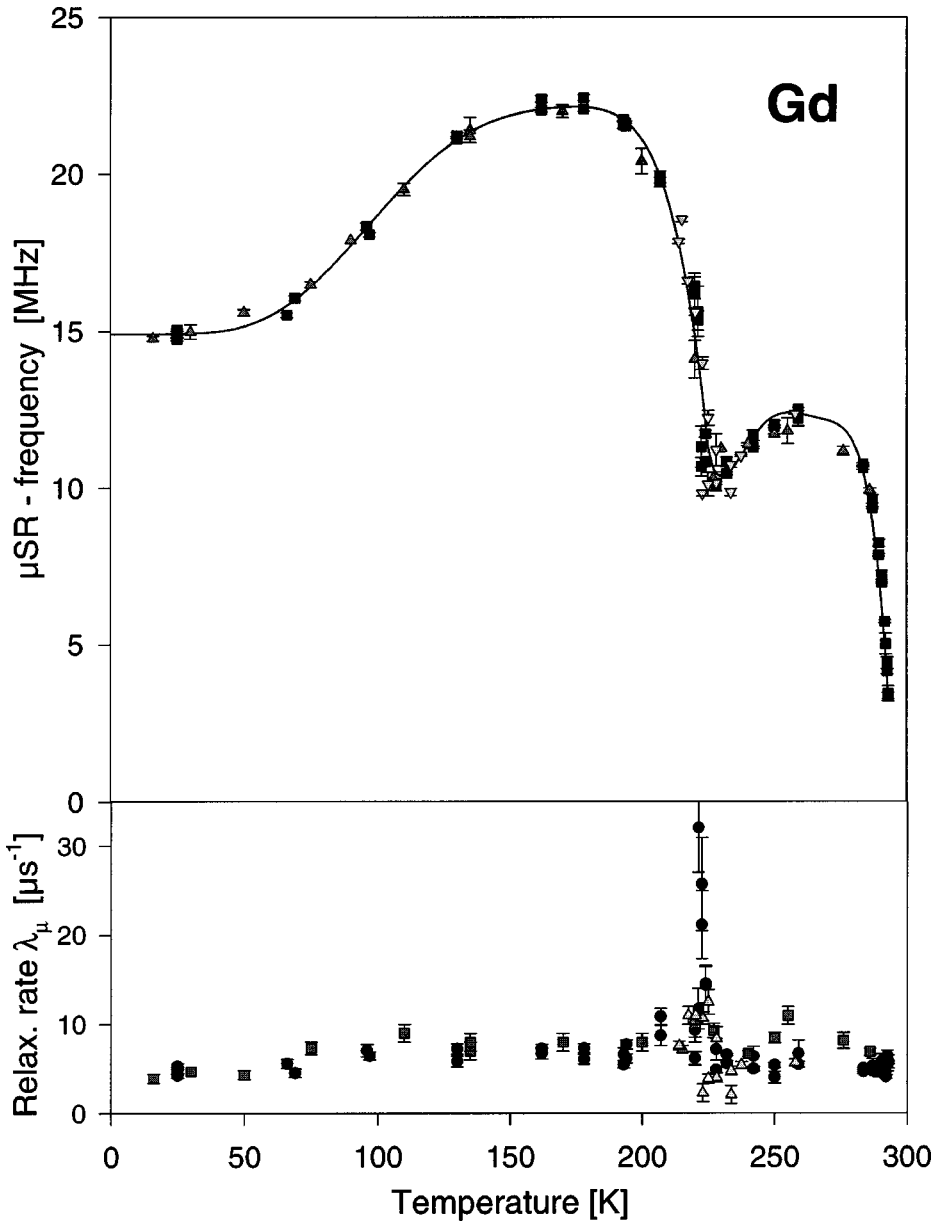

Figure 9. Temperature dependence of the spontaneous spin precession frequency ($\propto B_\mu$) in ferromagnetic Gd at ambient pressure. The peculiar shape is due to a tilting of spins out of the c-axis starting about 70 K below T_C (see text). The lower panel shows the relaxation rate λ_T as a function of temperature.

between 170 and 50 K. It is quite remarkable that the angle finally decreases again rather sharply on further reducing the temperature. The same same low temperature limit of $\sim 30^\circ$ is reached at all pressures.

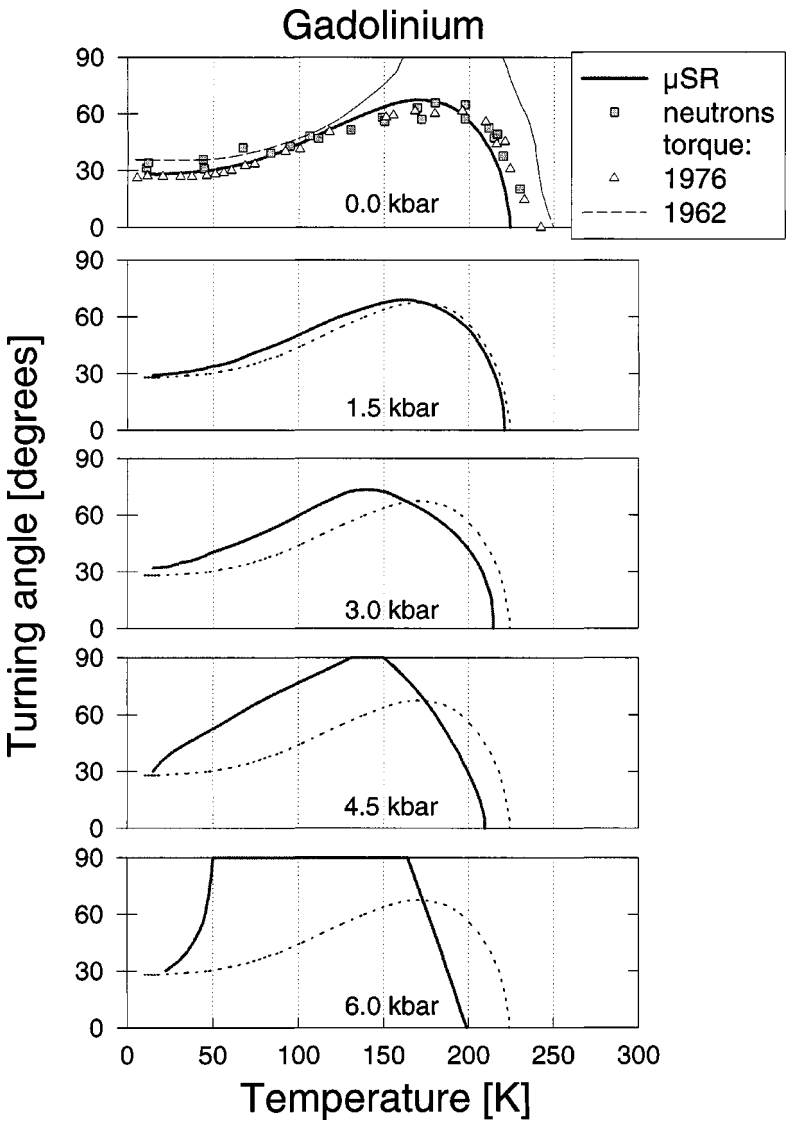

Figure 10. Spin turning angle Θ (with respect to the c-axis) in ferromagnetic Gd metal as a function of temperature for ambient (top) and applied pressures derived from the temperature variation of the internal field as shown in figure 9. Results from other measurements at ambient pressure are shown for comparison in the top panel. The panels depicting the results at applied pressures also contain the data for ambient pressure (dotted line) to make the differences more apparent.

4.2. Critical behavior of Gd

Measurements of the muon spin relaxation rate close, but still above, T_C taken in ZF under ambient conditions [18] have been compared to calculations based on mode coupling theory [19]. The result is shown in figure 11. One finds very good agreement.

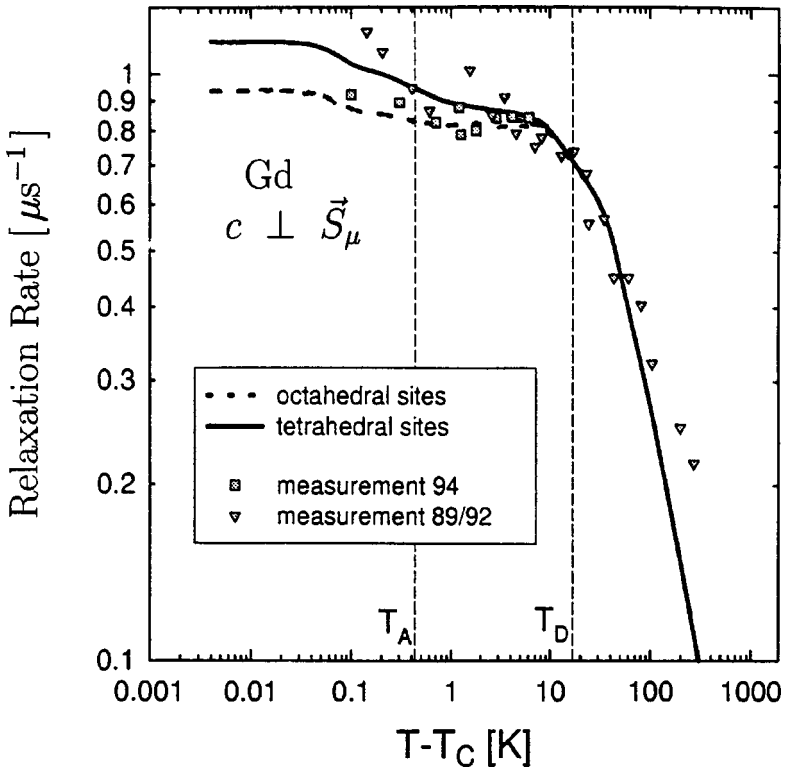

Figure 11. Comparison of the temperature dependence of the relaxation rate of Gd in the critical regime just above T_C together with the prediction of mode-coupling theory. The calculations were carried out for two possible muon stopping sites.

Two crossover points are seen. For $T - T_C > 10$ K Gd behaves like an isotropic Heisenberg FM. Below the first crossover point (i.e., for 1 K $< T - T_C <$ 10 K) dipolar anisotropy comes into play. Below the second crossover at $T - T_C = 1$ K uniaxial anisotropy has to be taken into account as well. These findings led to the definition of a new universality class.

High pressure measurements are easier performed in TF. Corresponding data on relaxation rate and muon Knight shift under ambient conditions had been reported in [20]. Figure 12 shows those data together with measurements under 6 kbar applied pressure. The first crossover point is clearly seen in both cases with no detectable change, indicating that the nature of the ferromagnetic phase transition does not change with small volume reductions.

4.3. The pressure dependence of the contact field in Gd, Ho, Dy

It appears that Ho is the simplest case and we shall discuss it first. Just below $T_N = 132$ K a helical AFM spin structure is stabilized. In lowering the temperature,

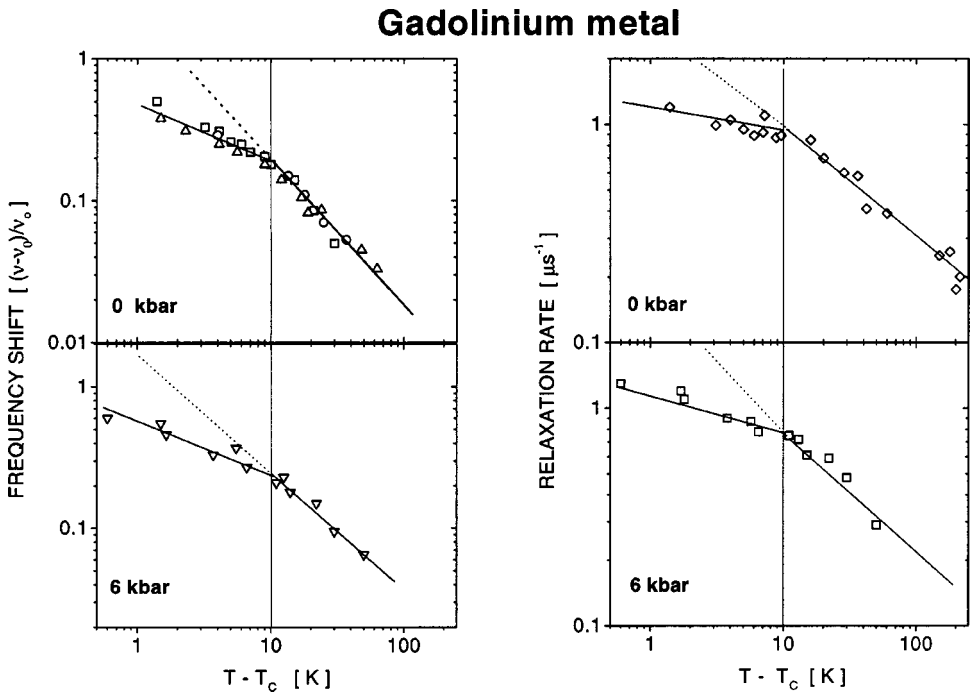

Figure 12. Temperature dependence of Knight shift and muon spin relaxation rate in paramagnetic Gd on approach to $T_{\rm C}$ at ambient and 6 kbar applied pressure. The lines are guides to the eye.

the helix becomes distorted, as can be seen from the appearance of higher harmonics in the neutron diffraction pattern. The magnetic order runs through a series of spin-slip structures until a second transition at $T_{\rm C} = 20$ K leads into a shallow-cone-shaped FM spin arrangement. The (fairly weak) net magnetization points along the c-axis. The helical component is commensurate, but the moments are not uniformly arranged, but are bunched around the b-axis. The cone angle decreases continuously towards 80° as $T \rightarrow 0$.

Muon spin precession is visible below $T_{\rm N}$. The temperature dependence of the precession frequency under ambient conditions is shown in figure 13. One finds an overall smooth and Brillouin-like variation of $\nu(T)$ in the AFM regime. Smaller deviations are seen in the vicinity of $T_{\rm C}$, where one also observes a splitting into two narrowly spaced frequencies. The probable cause is the spin–slip structure. Unusual, and still unexplained, is the decrease of local field B_μ in the FM regime where one expects $\nu(T) \approx$ const since the spin lattice magnetization should be saturated. A first thought is that a change in cone angle might be responsible. Dipolar field calculations failed to reproduce the effect for any sensible values. Furthermore, the same effect is seen in Dy (see figure 17), which possesses a simple FM structure. We can only offer at this stage the speculative explanation that, on account of the strong magnetic anisotropy, the bulk magnetization is not zero even in ZF cooling. The reduction of local field is then due to the presence of a demagnetization field.

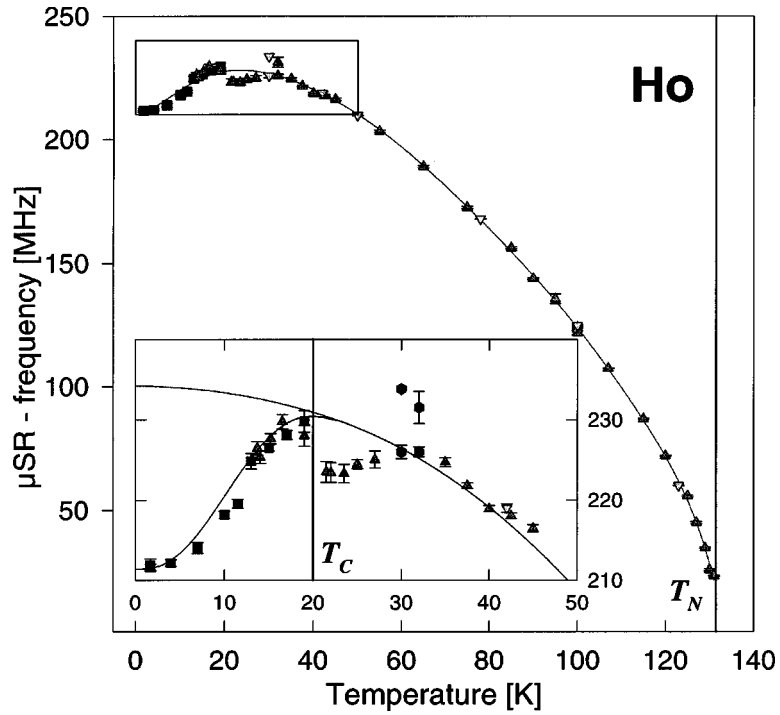

Figure 13. Temperature dependence of the spontaneous muon spin precession frequency (internal field) for (single crystalline) Ho. The inset shows details around the Curie temperature. Just above T_C two frequencies are observed, probably due to spin–slip behavior. The lines are guides to the eye.

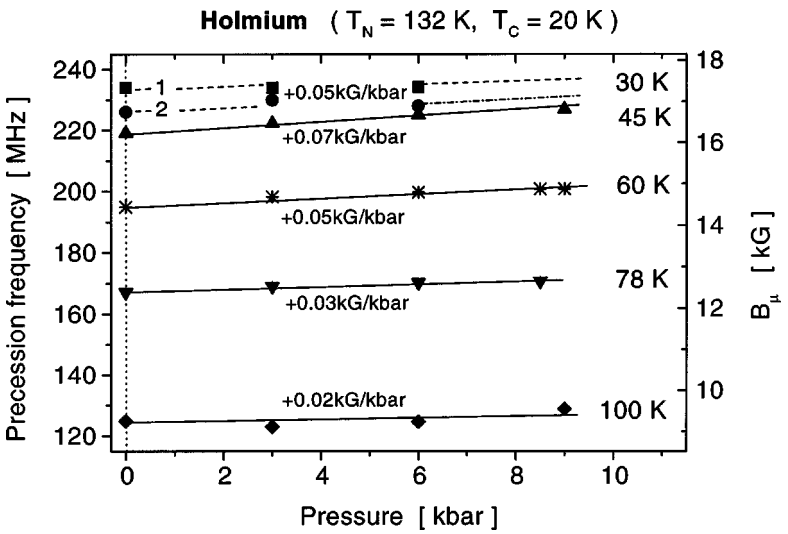

Figure 14. Pressure dependence of the precession frequency (local field) in antiferromagnetic Ho at different temperatures. The numbers give the pressure coefficients $\mathrm{d}B_\mu/\mathrm{d}p$ obtained from the linear regression fits shown as solid lines.

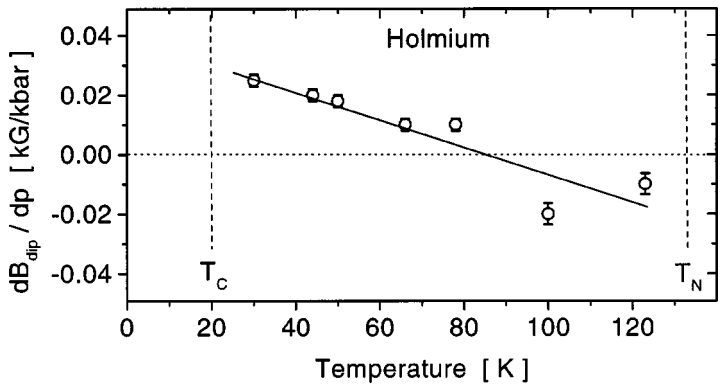

Figure 15. Plot of the calculated pressure coefficient of the dipolar field for Ho as a function of temperature.

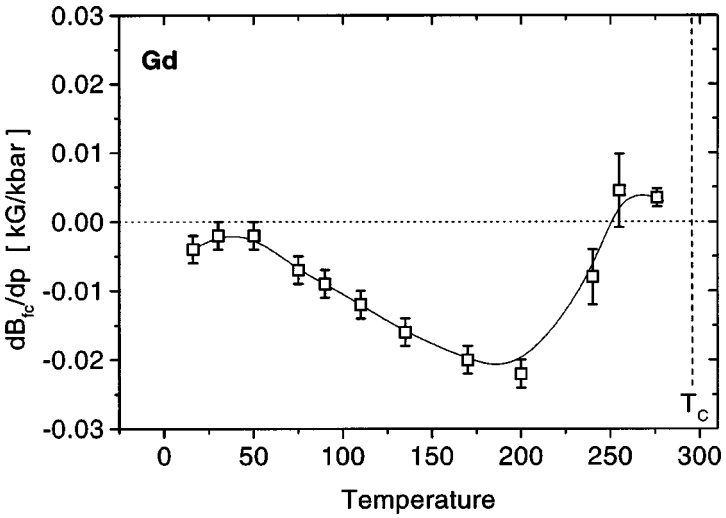

Figure 16. Temperature dependence of the pressure coefficient of the contact field in ferromagnetic Gd as derived from the measured pressure dependence of B_μ and the calculated pressure dependence of $B_{\rm dip}$ taking spin turning into account. The line is a guide to the eye.

The local field B_μ changes with applied pressure. The dependence of the local field on pressure is shown in figure 14 for various temperatures (all in the AFM regime since the high pressure spectrometer was limited in temperature to $T > T_{\rm C}$). According to eq. (7) we can treat the situation as the pressure changes of $B_{\rm dip}$ and $B_{\rm c}$. The situation is simple since the two fields are parallel. The change of $B_{\rm dip}$ can be calculated from the known pressure dependences of the transition temperatures and magnetic moments. Figure 15 presents the result for $\mathrm{d}B_{\rm dip}/\mathrm{d}p$ as a function of temperature. This allows to evaluate $\mathrm{d}B_{\rm c}/\mathrm{d}p$, which is the quantity of interest since it cannot be calculated straightforwardly. In the case of Ho one finds a value of $(+0.04 \pm 0.01)$ kG/kbar independent of temperature.

In Gd the measured dependence of B_μ on pressure and the calculated values of $\mathrm{d}B_{\mathrm{dip}}/\mathrm{d}p$ are complex because of the turning of spins. Plots corresponding to figures 11 and 12 make little sense. But the same technique used to extract the behavior of the tilt angle can be used to derive $\mathrm{d}B_{\mathrm{c}}/\mathrm{d}p$. Its dependence on temperature is depicted in figure 16 and shows a more complex behavior than in the case of Ho. It is remarkable that the change from a decrease to a rise in $\mathrm{d}B_{\mathrm{c}}/\mathrm{d}p$ occurs at the spin turning transition.

A large axial anisotropy confines the moments on Dy to the basal plane. Between $T_{\mathrm{N}} = 178$ K and $T_{\mathrm{C}} = 85$ K, a helical AFM spin structure is present. The helix angle decreases with lower temperature. At T_{C}, an orthorhombic distortion of the hcp lattice occurs and the transition into the FM state is of first order. The spins all have the same magnitude and all point along the orthorhombic a-axis, so this is a simple FM structure.

Data for the temperature dependence of the precession frequency under ambient pressure are shown in figure 17. As mentioned, a decrease of frequency is observed in the FM state like in Ho. Figure 18 presents the variation of B_μ with pressure for different temperatures (data in the vicinity of T_{C} were omitted because the transition temperature is also pressure dependent). It appears that at higher temperatures there is no uniform slope for $B_\mu(p)$ and we separate $\mathrm{d}B_\mu/\mathrm{d}p$ into two ranges, one below $\sim$3 kbar, the other above. The calculated variation of $\mathrm{d}B_{\mathrm{dip}}/\mathrm{d}p$ is again smooth

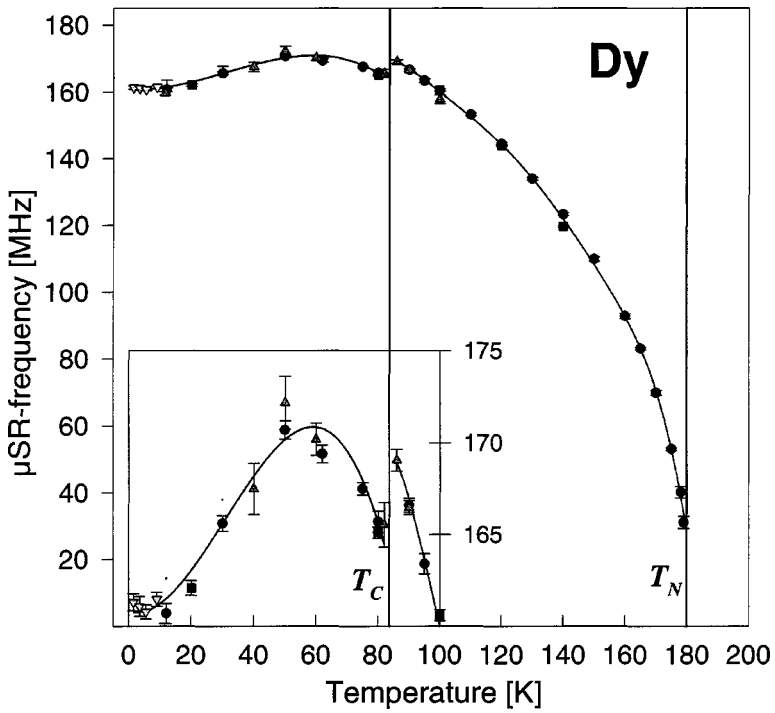

Figure 17. Temperature dependence of the spontaneous muon spin precession frequency (local field) in ferro- and antiferromagnetic (single crystalline) Dy. Details around T_{C} are shown in the inset. The lines are guides to the eye.

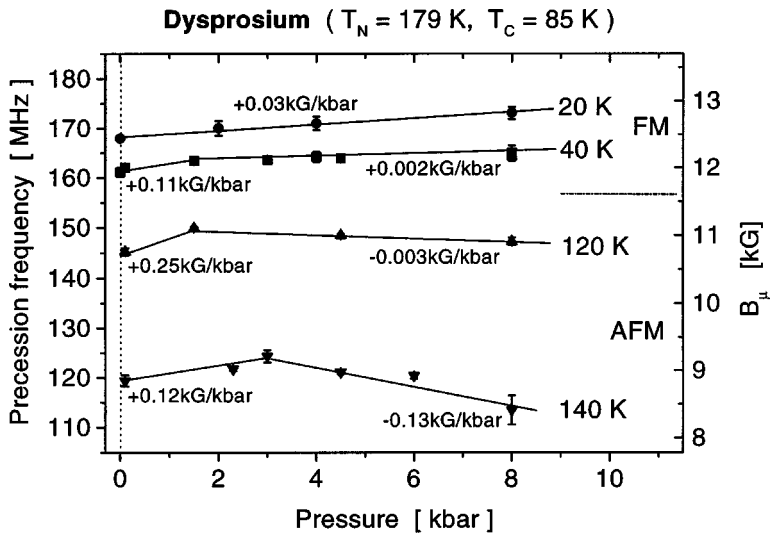

Figure 18. Pressure dependence of μSR frequency (local field) in ferro- (FM) and antiferromagnetic (AFM) Dy excluding the transition region. The numbers are the pressure coefficients $\mathrm{d}B_\mu/\mathrm{d}p$ derived from the linear regression fits shown as solid lines. Different slopes were fitted to the lower and higher pressure regions except for $T = 20$ K.

(figure 19, top). No change occurs at T_C since the moments are always confined to the basal plane. This then leads to the truly complex result for $\mathrm{d}B_\mathrm{c}/\mathrm{d}p$ shown in figure 19, bottom.

As mentioned, the calculation of the magnitude of B_c from first principles is difficult. Attempts have been made to explain the temperature dependence of B_c in the transition metals Fe, Co, Ni, but without striking success. Even correcting for thermal expansion using high pressure data brought only moderate improvement. Details can be found in [21]. For the rare earth metals such calculations do not exist to our knowledge. The data presented here show that the situation concerning the compressibility of the conduction electron sea is not simple and not uniform throughout the heavy rare earths. It definitely calls for more theoretical work.

5. YMn_2 and $GdMn_2$

The $REMn_2$ (RE = rare earth) series exists as Laves phase for practically all rare-earth atoms. The cubic (C15) variant is formed in the majority of cases. These compounds exhibit two special features with respect to their magnetic behavior. Firstly, the Mn atoms carry a moment only if the lattice parameter exceeds 7.6 Å (or the Mn–Mn separation 2.67 Å). Secondly, since the Mn ions form a sublattice of regular tetrahedrons, dominant nearest neighbor antiferromagnetic exchange leads to full geometrical frustration. Frustrated systems cannot support a collinear antiferromagnetic spin structure. YMn_2, however, combines the Néel transition with strong lattice ex-

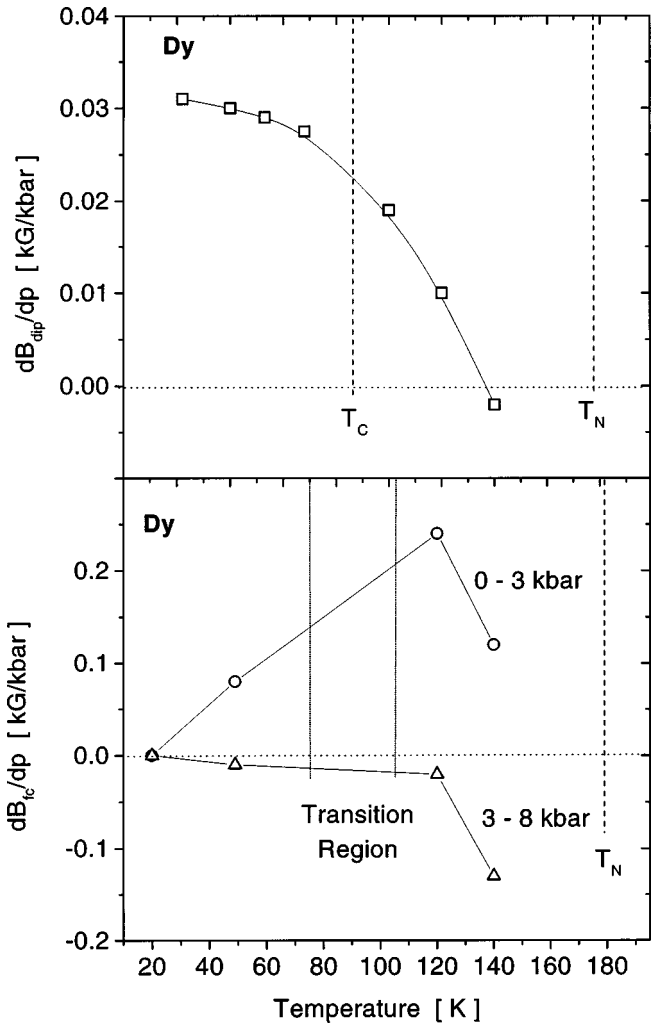

Figure 19. Calculated pressure coefficient of $B_{\rm dip}$ (top) and derived pressure coefficient of $B_{\rm c}$ (bottom). The lines are guides to the eye.

pansion ($\sim$5% volume change) and tetragonal distortion. This weakens the frustrating effect of nearest-neighbor exchange and makes the phase transition first order with a pronounced hysteresis. In addition, a long wave ($\sim$400 Å) helical modulation of the basically collinear spin structure is present.

The hysteresis at $T_{\rm N}$ is clearly seen in μSR. The Néel transition can be traced in TF measurements via the loss of signal amplitude, as mentioned above. Figure 20 presents the situation for YMn_2 at ambient pressure. The study of the pressure dependence of the magnetic transition was performed on a sample of $Y_{0.9}Tb_{0.1}Mn_2$. The addition of Tb slightly shifts the transition point and suppresses the helical spin modulation. The effect of pressure on $T_{\rm N}$ is dramatic as demonstrated by figure 21.

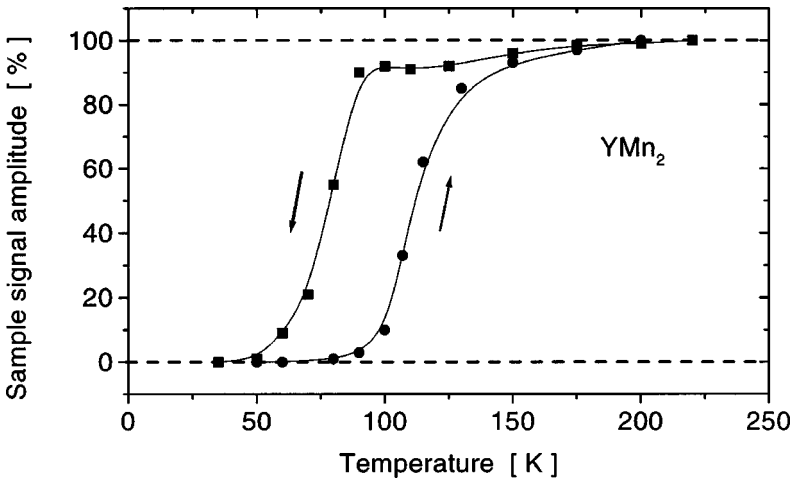

Figure 20. Trace of the Néel transition with its hysteresis by TF-μSR for YMn_2 at ambient pressure. The lines are guides to the eye.

The left panel shows the signal amplitude, the right panel the muon spin relaxation rate as a function of temperature. In the ordered state only a low intensity residual signal is seen which has a much reduced relaxation rate when compared to the paramagnetic state. In earlier work [22] it was argued that this residual signal arises from a portion of the sample which undergoes only short range order as a result of frustration. From the data presented in figure 21 one deduces the huge pressure coefficient $\mathrm{d}T_\mathrm{N}/\mathrm{d}p \approx -30$ K/kbar. The result agrees with resistivity measurements [23]. This leads to a critical pressure of $\sim$4 kbar for the disappearance of long-range order. Figure 22 gives further evidence in this direction. It shows the pressure dependence of the signal amplitude for two temperatures. At 20 K (our base temperature) the full AFM state only exists for $p < 1$ kbar. Bulk data also show that the Sommerfeld constant increases with pressure. This has led to the view that under pressures exceeding 4 kbar, one might regard YMn_2 as a $3d$ itinerant electron heavy Fermion material [24]. One can stabilize a non-AFM YMn_2 material by the addition of 3% Sc. This reduces the lattice constant and lattice pressure suppresses the Néel transition. μSR studies [25,26] have shown that only spin-glass-like short range order exists in this material for $T < 2$ K. Unfortunately, the present high pressure system does not allow measurements at such low temperatures.

RMn_2 compounds with RE other than Y have two magnetic sublattices. The RE sublattice does not have the strict triangular correlation of the Mn sublattice and is basically not frustrated. In $GdMn_2$ the Mn–Mn separation (and with it the Mn moment of $\sim 2.7\mu_\mathrm{B}$) is about the same as in YMn_2. The fact that Gd^{3+} is an S state ion leads to comparatively small magnetic anisotropy and an insensitivity to CEF interactions. A first magnetic transition at $T_\mathrm{N} = 104$ K is connected to a small volume change ($\sim$1%), but not to tetragonal distortion. Specific heat confirms its first order nature, but sees in addition a broad anomaly around 40 K. Magnetization data show ferromagnetic

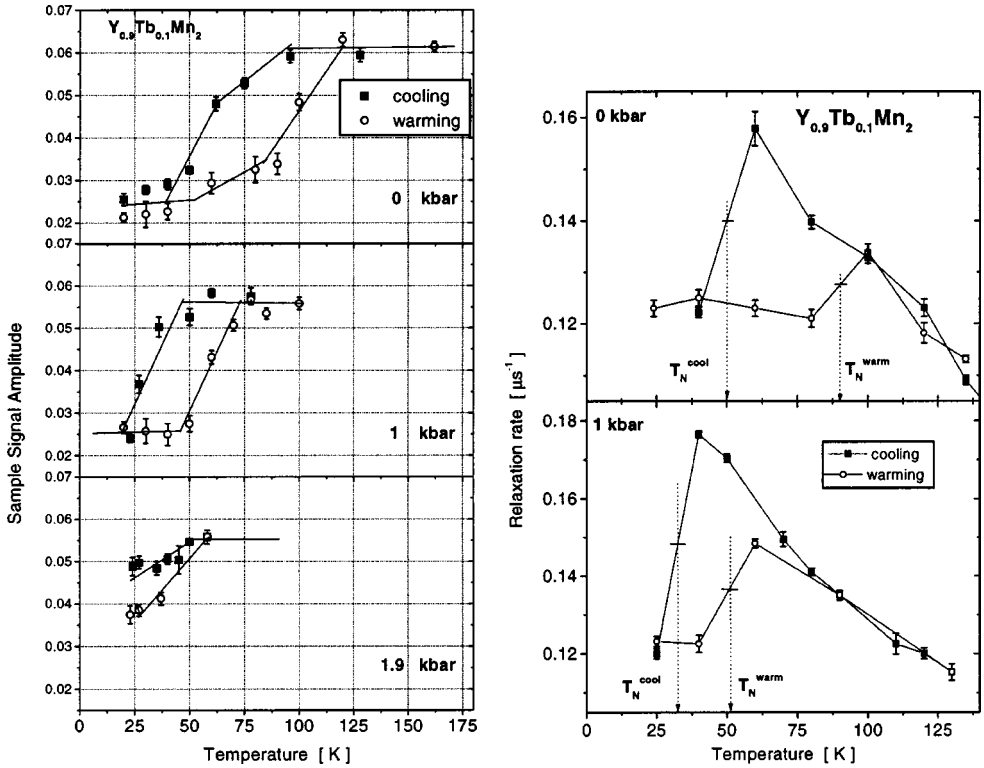

Figure 21. Temperature dependence of paramagnetic TF signal amplitude (a) and of relaxation rate (b) for $Y_{0.9}Tb_{0.1}Mn_2$ at different pressures. The lines are guides to the eye. Note that the width of hysteresis becomes smaller with pressure.

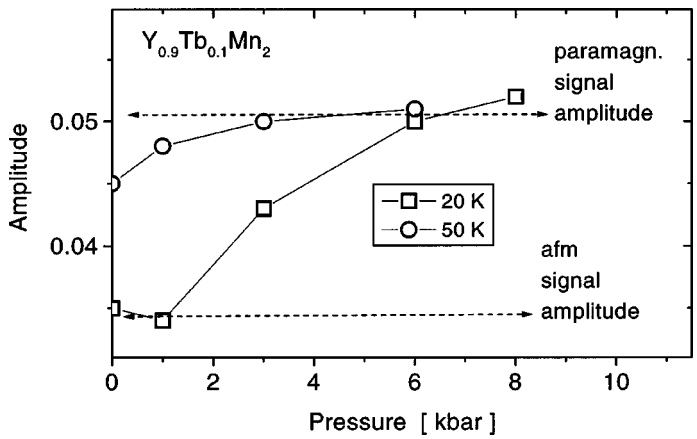

Figure 22. Pressure dependence of the TF amplitude at two temperatures for $Y_{0.9}Tb_{0.1}Mn_2$. The lines are guides to the eye.

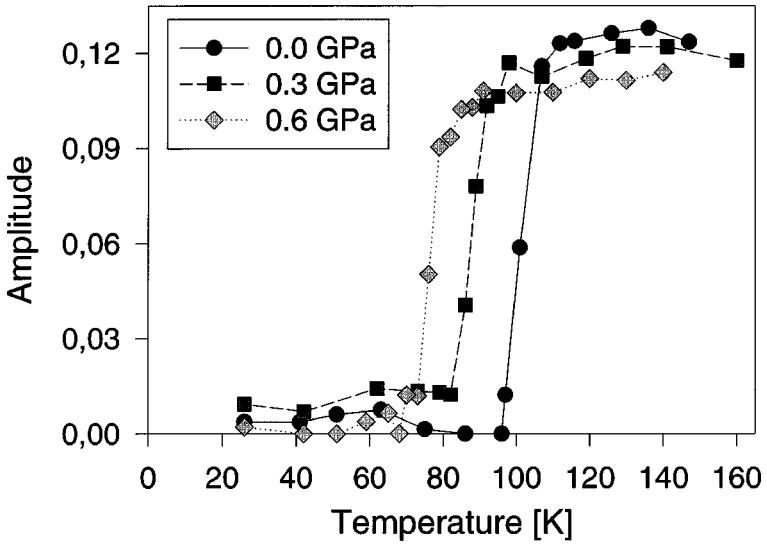

Figure 23. Temperature dependence of the TF signal amplitude for $GdMn_2$ at different pressures. The lines are guides to the eye.

behavior below 40 K. For this reason 40 K is often referred to as the Curie point (T_C) of $GdMn_2$. μSR studies at ambient conditions have shown conclusively, however, that a FM component already exists below T_N and that T_C should be considered a spin reorientation transition [27].

Our prime interest was to compare the pressure coefficient of T_N for YMn_2 and $GdMn_2$. Data similar to those shown in figure 21 for YMn_2 are presented in figure 23. Again a downshift of T_N with reduced volume is seen, but it is much smaller than in YMn_2, giving only $dT_N/dp \approx -5$ K/kbar. This result verifies resistivity data [23]. The final result is that the presence of the Gd magnetic sublattice reduces the effect of Mn moment destabilization. The μSR data at ambient pressure [27] further show that frustration is considerably reduced in $GdMn_2$ when compared to YMn_2. The main reason is the presence of an additional magnetic sublattice.

The critical behavior on approach to T_N from the paramagnetic side was also studied for $GdMn_2$. The relaxation rate $\lambda(t)$ is expected to follow a critical power law:

$$\lambda \propto \left[\frac{T - T_N}{T_N}\right]^{-w}. \tag{13}$$

This notion is well fulfilled at ambient conditions and under pressure, as demonstrated by the data shown in figure 24. One only observes a slight change of critical exponent w with pressure and concludes that the magnetic phase transition is shifted in temperature but keeps its basic nature under small volume reductions.

Finally, we mention, without going into details, that the high pressure μSR spectra point towards changes in the ordered spin structure of $GdMn_2$ with volume. In

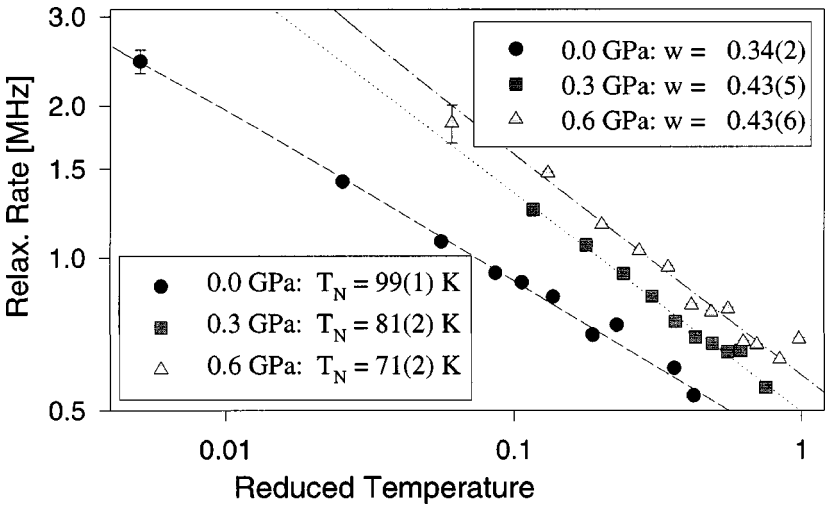

Figure 24. Temperature dependence of μSR relaxation rate in the paramagnetic critical regime of $GdMn_2$ at different pressures as a double logarithmic plot. The lines are fits to a critical power law. The fit parameters are given in the inset.

particular, variations of the FM component below T_N and also below T_C are observed together with the indication of an upward shift of T_C.

6. La_2CuO_4

The stoichiometric material La_2CuO_4 is the endpoint of the series $La_{2-x}(Sr,Ba)_x CuO_4$ which started the field of high T_C superconductivity. Optimally doped materials possess transition temperatures up to ~36 K. La_2CuO_4 is an antiferromagnetic insulator devoid of a superconducting transition. ZF-μSR measurements at ambient pressure in the AFM regime show a spontaneous spin precession pattern with $\nu = 5.6$ MHz. The corresponding local field is thought to arise solely from the dipolar fields of the AFM ordered Cu^{2+} moments. It was argued in [28] that contact fields may play an important role. With a pressure induced compression of the lattice constant of ~0.003 Å/kbar even moderate pressures should then affect B_c markedly. High pressure measurements up to 5 kbar were carried out at various temperatures within the AFM range. Figure 25 shows the dependence of the spontaneous precession frequency at $T = 10$ K. No effect of pressure on the μSR spectra was observed meaning that neither the local field B_μ nor the magnetic transition temperature T_N is affected by the induced reductions in volume. This questions the importance of the contact field as proposed in [28]. It also shows that the variation of volume on doping with Sr or Ba has hardly any influence on the suppression of AFM order. Essential for the move from ordered magnetism to superconductivity is the increase of charge carrier density.

We may add that this work also served as a case study for the use of powder material in the high pressure cell. A clear spectrum (see figure 26) was seen with

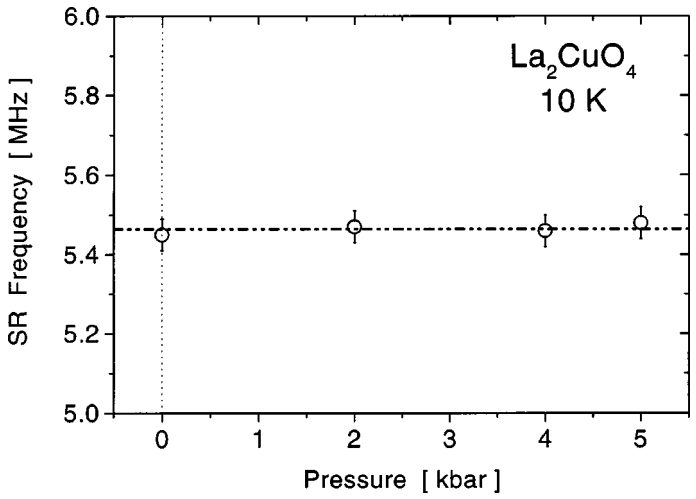

Figure 25. The spontaneous muon spin precession frequency in antiferromagnetic La_2CuO_4 at 10 K as a function of pressure.

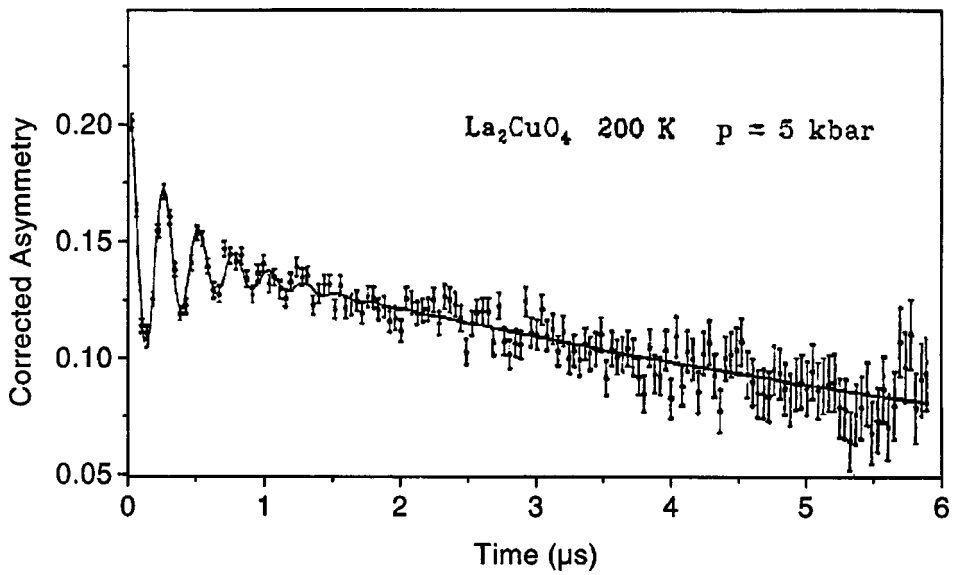

Figure 26. High pressure μSR spectrum of La_2CuO_4 showing the spontaneous spin precession signal of the sample riding on the slowly relaxing signal from muons stopped in the cell wall. A comparison with figure 8 shows that spectra of comparable quality can be obtained with a powder sample (La_2CuO_4) and a single crystal (Gd).

a relative amplitude of 35% for the oscillatory signal from the sample. The slowly varying signal comes from muons stopped in the cell walls. The possibility to work with powder samples was successfully demonstrated.

7. Outlook

The μSR gas pressure system operates well down to He temperatures and for pressures up to $\sim$10 kbar. There is of course the desire to go to lower temperatures and higher pressures, the former clearly having priority. With a gas pressure system the high pressure cell is too bulky to be cooled by a ^{3}He cryostat or a dilution refrigerator. One has to move towards smaller, more conventional high pressure cell designs, like systems used in neutron scattering work, since the demands on sample size are rather similar. At PSI the proton beam has been intensified to 1.5–2 mA in connection with the construction of a spallation neutron source at this facility. This allows in principle a narrowly collimated muon beam with sufficient intensity. But collimation of muon beams is not without problems and another serious question is whether the deviation from strict hydrostatic conditions still allows the recording of useful μSR spectra. Design and feasibility studies in this direction are under way in connection with the new cell design depicted in figure 27. It has been provided by M. Abd-Elmguid (University of Köln). We are confident that in the not too distant future a new high pressure apparatus will be available covering, in particular, the temperature and pressure ranges needed for the study of magnetic instabilities in highly correlated electron systems such as heavy fermion materials.

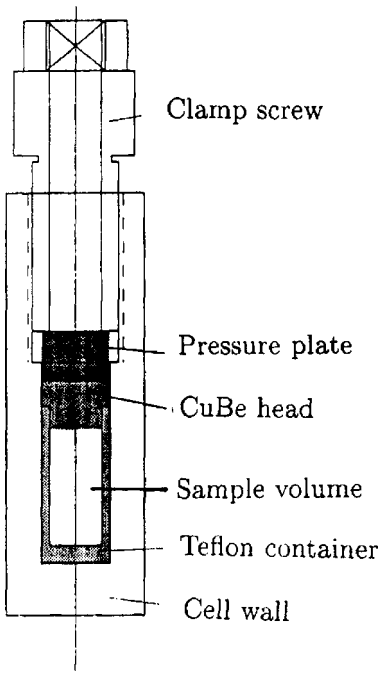

Figure 27. Outlay of a new high pressure cell. This is a piston-cylinder clamp cell device which has to be pressure loaded externally. The pressure is retained by tightening the clamp screw.

References

[1] A. Amato, Rev. Mod. Phys. 69 (1997) 1119.
[2] Y.J. Uemura, Hyp. Interact. 105 (1997) 35.
[3] T. Butz, G.M. Kalvius, B. Lindgren, O. Hartmann, R. Wäppling and E. Karlsson, Hyp. Interact. 32 (1986) 881.
[4] Th. Stammler, T. Grand, A.B. Kaiser, J. Major, A. Röck, R. Scheuermann, L. Schimmele and A. Seeger, Hyp. Interact. 104 (1997) 331.
[5] A. Schenck, A. Amato, F.N. Gygax, M. Pinkpank, A. Jung, P. Wachter, J. Major, Th. Stammler and R. Scheuermann, Hyp. Interact. 104 (1997) 209.
[6] A. Schenck, *Muon Spin Rotation Spectroscopy* (Adam Hilger, Bristol, 1985).
[7] J.H. Brewer, in: *Encyclopedia of Applied Physics*, Vol. 11 (VCH, New York, 1994) p. 23.
[8] O. Hartmann, E. Karlsson, R. Wäppling, J. Chappert, A. Yaouanc, L. Asch and G.M. Kalvius, J. Phys. F 16 (1986) 1593.
[9] R. Kubo, Hyp. Interact. 8 (1980/81) 739.
[10] B. Lindgren, O. Hartmann, E. Karlsson, R. Wäppling, T. Butz and G.M. Kalvius, Hyp. Interact. 31 (1986) 439.
[11] T. Butz, J. Chappert, J.F. Dufresne, O. Hartmann, E. Karlsson, B. Lindgren, L.O. Norlin, P. Podini and A. Yaouanc, Phys. Lett. A 75 (1980) 321.
[12] A. Kratzer, K. Mutzbauer, S. Henneberger, G.M. Kalvius, O. Hartmann, R. Wäppling, H.-H. Klauß, M.A.C. De Melo, F.J. Litterst and Th. Stammler, Hyp. Interact. 87 (1994) 1055.
[13] A.B. Denison, H. Graf, W. Kündig and P.F. Meier, Helv. Phys. Acta 52 (1979) 460.
[14] O. Hartmann, E. Karlsson, R. Wäppling, L. Asch, S. Henneberger, G.M. Kalvius, A. Kratzer, H.-H. Klauß, F.J. Litterst and M.A.C. De Melo, Hyp. Interact. 85 (1994) 251.
[15] J.W. Cable and E.O. Wollan, Phys. Rev 165 (1968) 733.
[16] W.D. Corner and B.K. Tanner, J. Phys. C 9 (1976) 627.
[17] C.D. Graham, Jr., J. Phys. Soc. Japan 17 (1962) 1310.
[18] S. Henneberger, E. Schreier, A. Kratzer, L. Asch, G.M. Kalvius, E. Frey, F. Schwabl, O. Hartmann, M. Ekström, R. Wäppling, F.J. Litterst and H.-H. Klauß, Hyp. Interact. 104 (1997) 301.
[19] E. Frey, F. Schwabl, S. Henneberger, O. Hartmann, R. Wäppling, A. Kratzer and G.M. Kalvius, Phys. Rev. Lett. 79 (1997) 5142.
[20] E. Wäckelgård, O. Hartmann, E. Karlsson, R. Wäppling, L. Asch, G.M. Kalvius, J. Chappert and A. Yaouanc, Hyp. Interact. 31 (1986) 325.
[21] B. Lindgren, O. Hartmann, E. Karlsson, R. Wäppling, A. Yaouanc, T. Butz, L. Asch and G.M. Kalvius, J. Magn. Magn. Mater. 67 (1987) 130.
[22] G.M. Kalvius, Hyp. Interact. 84 (1994) 249.
[23] R. Hauser, A. Indinger, E. Bauer and E. Gratz, J. Magn. Magn. Mater. 140–144 (1995) 799.
[24] C. Lacroix and C. Pinettes, Phys. B 206/207 (1995) 11.
[25] M. Mekata, T. Asano, H. Nakamura, M. Shiga, K. Kojima, G.M. Luke, A. Keren, W.D. Wu, Y.J. Uemura, S. Dunsiger and M. Gingras, Hyp. Interact. 104 (1997) 337.
[26] G.M. Kalvius, M. Weber, A. Kratzer, E. Schreier, R. Ballou, J. Deportes, R. Wäppling, J. Chappert and F.J. Litterst, in: *Proc. of Internat. Conf. HFI* (1995), Hyp. Interact. C 1 (1996) 135.
[27] G.M. Kalvius, E.M. Martin, E. Schreier, A. Kratzer, O. Hartmann, R. Wäppling, D.R. Noakes, K. Krop, R. Ballou and J. Deportes, Phys. B, to be published.
[28] R. Saito, H. Kamimura and K. Nagamine, Phys. C 185 (1991) 1217.